An X-ray Powder Diffraction Study of the Microstructure and Growth Kinetics of Nanoscale Crystallites Obtained from Hydrated Cerium Oxides

Nathalie Audebrand, Jean-Paul Auffrédic, and Daniel Louër*

Laboratoire de Chimie du Solide et Inorganique Moléculaire (U.M.R. C.N.R.S. 6511), Groupe de Cristallographie des Poudres et Réactivité des Solides, Avenue du Général Leclerc, 35042 Rennes Cedex, France

Received February 8, 2000. Revised Manuscript Received March 7, 2000

A detailed analysis of the microstructural properties of nanocrystalline cerium(IV) oxide powders produced by thermal dehydration of two hydrated ceria precipitated from the ceric ammonium and sulfate salts in ammonia solutions is described. In addition, it is shown that the diffraction pattern of hydrated ceria can be modeled with the structure data of CeO_2 and that the average crystallite size for the precursor $CeO_2 \cdot 1.6H_2O$ is 19 Å. The analysis of nanocrystalline CeO_2 is based on the modern developments of X-ray powder diffraction line broadening analysis, using 16 Bragg reflections. It is shown that, on average, the crystallites have a spherical shape with volume-weighted and area-weighted diameters in the ranges 264−1349 Å and 178−1079 Å for CeO_2 (*am*-CeO_2) obtained from the ammonium-based ceria and 263−1756 Å and 195−927 Å for CeO_2 (*sul*-CeO_2) obtained from the sulfate-based ceria. The early stages of the crystallite growth have been studied up to 775 °C and 900 °C, respectively. While *sul*-CeO_2 is strain-free over the temperature range investigated, *am*-CeO_2 contains a small amount of strains decreasing with temperature until 700 °C, where strains are negligible. The kinetics of the crystallite growth has been studied for the two samples, from which activation energies have been calculated. Crystallite sizes are also compared to the values from SEM and BET measurements. Strain-free *sul*-CeO_2 is suggested as a potential candidate as reference material for crystallite size in powder diffraction.

1. Introduction

There is an increasing interest in the chemistry and physical properties of nanoscale "particles" in technologically important applications. In particular materials with high surface area have an importance in two major fields, those of ceramic science and heterogeneous catalysis. There are many synthetic routes to high surface area oxides, e.g., thermal decomposition of inorganic precursors, gas condensation, precipitation from solutions. In particular, inorganic precursors with low thermal stability, e.g., nitrates, oxalates, and acetates, can produce nanocrystalline powders at low temperatures (150−200 °C). A few examples in which X-ray diffraction line broadening analysis was used to characterize precisely the microstructure of nanocrystalline powders have been reported in the literature. Representative examples are ZnO samples prepared from nitrate-, oxalate-, acetate-, and carbonate-based precursors,[1−3] CeO_2 prepared from the oxide nitrate[4] or from gas condensation,[5] CuO and ZnO obtained from basic salts.[6] Among these examples, the thorough study on four nanocrystalline ZnO powders[3] as a function of temperature has clearly shown that the microstructural properties (crystallite size and shape, strain, stacking faults) of the oxide were governed by the chemical nature of the precursor, demonstrating the existence of some sort of "genetic" relationships. Generally, varied techniques are used to characterize the particles in loose powders, such as electron microscopy, gas adsorption and X-ray diffraction line broadening analysis. The last method leads to a unique characterization in the sense of coherently diffracting domains (denoted here crystallites), measurable in the approximate range 2−100 nm. While a gross evaluation of the sizes, based on the Scherrer equation often applied to only one reflection, is frequently reported in studies on nanocrystalline oxides, precise characterization of the microstructure from line-broadening analysis can now be carried out from the recent advances combining pattern-fitting techniques and the methods based on the integral breadth and Fourier methods (e.g., ref 7). With this approach all diffraction lines in the pattern are analyzed, from which a three-dimensional description of the

* To whom correspondence should be addressed. E-mail address: Daniel.Louer@univ-rennes1.fr. Fax: (33) 2 99 38 34 87.

(1) Louër, D.; Auffrédic, J. P.; Langford, J. I.; Ciosmak, D.; Niepce, J. C. *J. Appl. Crystallogr.* **1983**, *16*, 183−191.
(2) Langford, J. I.; Boultif, A.; Auffrédic, J. P.; Louër, D. *J. Appl. Crystallogr.* **1993**, *26*, 22−33.
(3) Audebrand, N.; Auffrédic, J.-P.; Louër, D. *Chem. Mater.* **1998**, *10*, 2450−2461.
(4) Guillou, N.; Auffrédic, J. P.; Louër, D. *Powder Diffr.* **1995**, 236−240.
(5) Guillou, N.; Nistor, L. C.; Fuess, H.; Hahn, H. *Nanostruct. Mater.* **1997**, *8*, 545−557.
(6) García-Martínez, O.; Rojas, R. M.; Vila, E.; Martín de Vidales, J. L. *Solid State Ionics* **1993**, *63*−*65*, 442−449.
(7) Langford, J. I.; Louër, D. *Rep. Prog. Phys.* **1996**, *59*, 131−234.

10.1021/cm001013e CCC: $19.00
Published on Web 05/04/2000

microstructural properties can be expected, as shown for instance for nanocrystalline ZnO powders obtained from various precursors.[1,3]

Cerium(IV) oxide is an example of a material where the number of applications has increased rapidly, e.g., as active material in catalytic converters, catalysts, ceramics. The present study deals with the characterization of nanocrystalline cerium oxide prepared from two hydrated ceria, $CeO_2 \cdot xH_2O$, obtained by precipitation from ammonia solutions of two precursors of cerium(IV), the sulfate and the ammonium nitrate. The use of Ce(IV) sulfate as precursor of finely dispersed CeO_2 has also been reported in precipitation processes based on forced hydrolysis, with a special attention to the characterization of monodispersed particles[8] and to the conditions to obtain ultrafine CeO_2 powders.[9] These purposes contrast with the aim of the present study based on the characterization of the diffracting domains constituting a "particle" (or a grain). Since there is no solid-state decomposition during the thermal treatment of the hydrated oxides, the microstructure of CeO_2 is free from any influence of structural phase transformation, which is a priori favorable for obtaining simple microstructures, i.e., dominated by crystallite size effects and a low strain content. This should differ from the microstructural properties of a number of CeO_2 powders obtained from the thermal decomposition of various nitrate-based Ce(IV) precursors, such as $Ce_2O(NO_3)_6 \cdot 8H_2O$,[4] $CeM_2(NO_3)_6$ (M = NH_4, K, Rb, Cs),[10,11] and $CeMg(NO_3)_6 \cdot 8H_2O$,[10] for which a significant amount of strains was found. In the present study, the crystal structure of hydrated ceria, and then its chemical nature, is also determined from the diffraction data set of a sample with the composition $CeO_2 \cdot 1.6H_2O$. The samples of CeO_2 obtained from dehydration of the two precursors have been heated isothermally at various temperatures and thoroughly analyzed from X-ray powder diffraction data collected at room temperature with the profile-fitting technique combined with the integral breadth and Fourier methods. The microstructural properties have been precisely determined and used to investigate the kinetics of the early stages of crystallite growth.

2. Experimental Section

2.1. Preparation of Ultrafine $CeO_2 \cdot xH_2O$. Two samples of ultrafine hydrated cerium oxide, $CeO_2 \cdot xH_2O$, were precipitated at room temperature from the addition of Ce(IV) salts (0.1 M), namely $(NH_4)_2Ce(NO_3)_6$ (Merck) and $Ce(SO_4)_2 \cdot 4H_2O$ (Merck), in a 1 M ammonia solution. The yellow precipitate of $CeO_2 \cdot xH_2O$ was washed with distilled water and with alcohol and then dried at room temperature. The chemical formula of these two samples was established from thermogravimetric analyses, i.e., $CeO_2 \cdot 4.3H_2O$ and $CeO_2 \cdot 1.6H_2O$ for the two samples obtained from $(NH_4)_2Ce(NO_3)_6$ and $Ce(SO_4)_2 \cdot 4H_2O$, respectively. Complete dehydration was achieved at 350 and 450 °C, respectively. In the following, the CeO_2 samples prepared from the dehydration of these two precursors are denoted as *am*-CeO_2 and *sul*-CeO_2. No trace of the precursors was detected in the precise powder diffraction patterns used in this study.

2.2. Preparation of Nanocrystalline CeO_2. The temperature range for which a precise characterization of the microstructure of a nanocrystalline solid can be performed from X-ray diffraction line broadening depends on the combined effects of the degree of line overlap and the magnitude of line broadening with respect to the instrumental contribution. The problems arise from the severe line broadening for samples prepared at low temperatures and from the instability of the instrumental correction when the intrinsic broadening is small compared to the instrumental contribution for samples annealed at high temperatures. Consequently, precise studies on *am*-CeO_2 and *sul*-CeO_2 samples were restricted to the temperature ranges 550−775 °C and 600−900 °C, respectively. Samples of *am*-CeO_2 and *sul*-CeO_2 were prepared from dehydration of 0.7 g of the precursors $CeO_2 \cdot 4.3H_2O$ and $CeO_2 \cdot 1.6H_2O$, under nitrogen, with heating rates of 100 and 170 °C h^{-1}, respectively, until the selected annealing temperature. To ensure a complete annealing at a given temperature and, then, a thermodynamically stable microstructure, samples were preserved at this constant temperature for times ranging from 1 day (higher temperatures) to a few days (lower temperatures) before being cooled at room temperature.

2.3. X-ray Diffraction Data Collection. Precise powder diffraction data of CeO_2 samples were obtained at room temperature with a Siemens D500 high-resolution powder diffractometer, using monochromatic Cu $K\alpha_1$ X-rays (λ = 1.5406 Å) obtained with a germanium incident-beam monochromator. The characteristics of this arrangement have been described elsewhere.[12] The diffraction patterns of CeO_2 (cubic symmetry, space group $Fm3m$, $a = 5.41129 \pm 0.00008$ Å[13]) were scanned over the angular range 23−148° (2θ). Step lengths and counting times were chosen according to line broadening, which decreases as the annealing temperature increases. Step lengths were selected to be approximately 1/10 of the fwhms, i.e., in the range 0.01−0.03° (2θ) until 83° (2θ) and in the range 0.03−0.07° (2θ) to the end of the scan. Counting times were selected in the range 20−120 s $step^{-1}$ until 83° (2θ) and 75−175 s $step^{-1}$ for the second section of the patterns. Instrumental line profiles were obtained by means of data from the standard reference material LaB_6 (μ = 1138 cm^{-1}, where μ is the linear absorption coefficient calculated with Cu $K\alpha_1$ radiation), marketed by NIST.[14] Eighteen reflections were recorded in the angular range 23−150° (2θ). Step lengths (∼fwhm/10), scan ranges (∼10−20 × fwhm), and counting times in the range 40−180 s $step^{-1}$ were adapted to the dispersion and intensity of each diffraction line. Furthermore, powder diffraction data for one precursor, $CeO_2 \cdot 1.6H_2O$, were collected over the range 20−147° (2θ) with a step length of 0.1° (2θ) and a counting time of 70 s $step^{-1}$.

The kinetic parameter n of the crystallite-growth kinetic was determined at a constant temperature from time-dependent X-ray diffraction (TDXD). It was carried out with an INEL (CPS 120) curved-position-sensitive detector, used in a diffraction geometry by reflection (Cu $K\alpha_1$ radiation) described elsewhere.[15] The stationary samples of $CeO_2 \cdot xH_2O$ were heated in a monitored high-temperature device. The samples were dehydrated at a constant heating rate of 350 °C h^{-1} up to 350 °C. Then a fast heating rate (∼1200 °C h^{-1}) was applied to reach the selected temperature. Because of the fast initial crystallite growth (as shown below) relatively short counting times, 300 s per pattern, were used.

2.4. BET and SEM Measurements. The specific surface areas, S_{BET}, of the CeO_2 powders were obtained using nitrogen adsorption at 77 K (Flowsorb II 2300 Micromeritics Instrument

(8) Hsu, W. P.; Rönnquist, L.; Matijevic, E. *Langmuir* **1988**, *4*, 31−37.
(9) Hirano, M.; Kato, E. *J. Mater. Sci. Lett.* **1996**, *15*, 1249−1250.
(10) Guillou, N. Ph.D. Thesis, University of Rennes, 1994.
(11) Audebrand, N. Ph.D. Thesis, University of Rennes, 1998.
(12) Louër, D.; Langford, J. I. *J. Appl. Crystallogr.* **1988**, *21*, 430−437.
(13) Standard Reference Material 674, 1983, National Institute of Standards and Technology (formely Natl. Bur. of Stand.), Gaithersburg, MD.
(14) Fawcett, T. G.; Crowder, C. E.; Brownell, S. J.; Zhang, Y.; Hubbard, C.; Schreiner, W.; Hamill, G. P.; Huang, T. C.; Sabino, E.; Langford, J. I.; Hamilton, R.; Louër, D. *Powder Diffr.* **1988**, *3*, 209−218.
(15) Plévert, J.; Auffrédic, J. P.; Louër, M.; Louër, D. *J. Mater. Sci.* **1989**, *24*, 1913−1918.

S.A.). The single point BET method was used to determine the surface area. Prior to analysis, samples were degassed at 400 °C for 1 h to eliminate adsorbed water. Scanning electron microscopy (SEM) observations were carried out by means of a JEOL SEM 6400 instrument.

2.5. Diffraction Line Broadening Analysis. The two approaches based on the integral breadth β and the Fourier methods have been used to determine the magnitude of strains and apparent crystallite sizes, ϵ_β and ϵ_F, which are defined as a volume-weighted size and an area-weighted size, respectively.[7] To investigate the microstructure of a sample, reliable parameters defining the position, the breadths fwhm, and integral breadth β (= integral intensity/peak height), the profile and shape of the diffraction lines are required. These quantities are easily extracted from pattern-modeling software, provided the counting statistics of the data are good enough and that line overlap is not too severe.[16] In this procedure the Bragg reflections are represented by analytical functions, which are fitted to the observed data by the method of least squares. The functions used are the Pearson VII, the pseudo-Voigt, and the Voigt, characterized by their shape factor, i.e., the exponent m, the mixing factor η, and ϕ (= fwhm/β), respectively. Additional details can be found elsewhere.[7] In the present study, pattern decomposition was carried out with the Socabim program PROFILE, which is a part of the DIFFRAC-AT package supplied by Siemens. The physical interpretation is clearly based on the analysis of the sample-dependent f profile, derived from the observed h profile after deconvolution by the instrumental profile g ($h = f * g$). The two methods (integral breadth and Fourier approaches) have been applied from the profile parameters extracted from PROFILE.

A. Integral-Breadth Methods. In the Langford method[17] a Voigt function is assumed to model adequately the observed h and g profiles, which means that the profiles are symmetrical and that the line-shape parameters ϕ lie within the Lorentzian limit ($\phi = 0.6366$) and the Gaussian limit ($\phi = 0.9394$). It should be noted that this simple method cannot be applied if data are markedly asymmetric or line shape is out of the Lorentzian (or Gaussian) limit. Observed β_h, obtained from PROFILE, were corrected for the instrumental contribution to give the integral breadth β_f of the f profiles in angular units (°2θ), and then converted to reciprocal units β_f^* (= $\beta_f \cos\theta/\lambda$). If line broadening is solely attributed to a size effect the apparent size ϵ_β (= β_f^{*-1}) is obtained. If structural distortions (microstrain) also contribute to line broadening, some approximations are required to separate the different effects.[17]

In the TDXD experiment the data quality was considerably poorer. Consequently, the line broadening analysis was limited to the integral breadth approach, using an approximation to the integral breadth of the Voigt function,[18] i.e., $\beta_h^2 \approx \beta_f\beta_h + \beta_g^2$, for the correction of the instrumental contribution.

B. Fourier Analysis. According to the Warren−Averbach−Bertaut[19] procedure, the Stokes' corrected cosine Fourier coefficients $A(n,l)$, where n is the Fourier harmonic number and l the order of reflection, of the sample-dependent line profile (f) can be expressed as the product of, order-independent, size coefficients $A^S(n)$ and, order-dependent, distortion coefficients $A^D(n,l)$. Considering a series expansion of $A(n,l)$, valid for low values of l and n, $A^S(n)$ and the microstrain $\langle e^2(n)\rangle$ can be separated, if at least two orders of a reflection are available. The Fourier coefficients are expressed as a function of a distance, perpendicular to the diffracting planes, $L = n/\Delta s$, where Δs [= $2(\sin\theta_2 - \sin\theta_1)/\lambda$, θ_1 and θ_2 are the limits of the angular range, and λ is the wavelength of the radiation] is the range, in reciprocal units, which contains all intensity points of the reflection. The initial slope of $A^S(n)$ versus L is generally a measure of the Fourier apparent size ϵ_F. The technique has been recently combined with profile fitting, through a new software *Prof*FOU,[20] for which applications have been reported elsewhere.[21] In this procedure line shape parameters (2θ, fwhm, m for the Pearson VII, η for the pseudo-Voigt) are extracted with PROFILE for both the observed h and instrumental g profiles. Then, they are employed to generate analytically the h and g profiles used in the Stokes Fourier deconvolution in order to obtain the Fourier coefficients of the f profile due to structure imperfections.

As indicated above the apparent sizes derived from Fourier (ϵ_F) and integral breadth (ϵ_β) have not the same definition.[22] Nevertheless, the two apparent measures can be related to the true size if the crystallite shape is known or assumed. For instance, for a spherical crystallite, the true diameter D is simply derived from $3\epsilon_F/2$ and $4\epsilon_\beta/3$, respectively. This relation is strictly valid for a monodisperse system. The presence of a size distribution introduces discrepancies between D_F and D_β.[23] In the present study, narrow size distributions are expected because precursors are subjected to controlled soft thermal conditions.

3. Microstructure of Nanocrystalline CeO_2

3.1. Crystallite Size of the Precursor $CeO_2 \cdot 1.6H_2O$. The X-ray diffraction patterns of the two precursors showed considerable broadening. To know the exact chemical nature of the highly hydrated precursors, the powder data of $CeO_2 \cdot 1.6H_2O$ have been carefully analyzed. Because of the extremely broad diffraction lines, which prevent a precise analysis of the individual lines, a whole pattern-modeling approach has been applied.

The procedure employed to model the powder diffraction pattern of $CeO_2 \cdot 1.6H_2O$ follows that described elsewhere[16] for simulated patterns of nanocrystalline ZnO. Crystallites were assumed to be isotropic and monodisperse. Various diameters D were selected in the range 10−25 Å. The apparent sizes ϵ_β (= 3D/4) were transformed into integral breadths β^* (= ϵ_β^{-1}), and then expressed in 2θ units $\beta_{2\theta}$ (= $\lambda\beta^*/\cos\theta$) for all lines hkl in the pattern. A Lorentzian function was selected to describe the diffraction line profiles. Patterns were generated (Cu Kα_1 wavelength) by means of the program POWDER CELL,[24] using the structure data of CeO_2. The angular dependence of fwhm was modeled by the quadratic form reported by Caglioti et al.,[25] from the fwhm values of the Lorentzian reflections calculated from the relation fwhm = $0.6366\,\beta_{2\theta}$, since the Lorentzian is a limit of the Voigt function.[7] At this stage, each simulated pattern was compared to the observed data with the Rietveld program FULLPROF.[26] In the calculation, the usual variable parameters were refined, except the structure model, the U, V, and W parameters of the Caglioti equation and the line shape. Each refinement was characterized by the R-weighted profile factor R_{wp}.[7] The refinements were found to be very sensitive to the simulated powder patterns, as shown

(16) Louër, D. *Adv. X-ray Anal.* **1994**, *37*, 27−35.
(17) Langford, J. I. In *Accuracy in Powder Diffraction II*; Prince, E., Stalick, J. K., Eds.; Spec. Publ. 846; NIST: Gaithersburg, MD, 1992; pp 110−126.
(18) Halder, N. C.; Wagner, C. N. J. *Adv. X-ray Anal.* **1966**, *9*, 91−102.
(19) Warren, B. E. *X-ray Diffraction*; Addison-Wesley: Reading, MA, 1969.
(20) Louër, D.; Audebrand, N. *Adv. X-ray Anal.* **1999**, *41*, 556−565; CD-ROM; ICDD: Newtown Square.
(21) Audebrand, N.; Louër, D. *J. Phys. IV Fr.* **1998**, *8*, 105−118.
(22) Guinier, A. *X-ray Diffraction*; Freeman: San Francisco, 1963.
(23) Langford, J. I.; Louër, D.; Scardi, P. *J. Appl. Crystallogr.* **2000**, in press.
(24) Kraus, W.; Nolze, J. *J. Appl. Crystallogr.* **1996**, *29*, 301−303.
(25) Caglioti, G.; Paoletti, A.; Ricci, F. P. *Nucl. Instrum. Methods* **1958**, *35*, 223−228.
(26) Rodriguez-Carvajal, J. In *Collected Abstract of Powder Diffraction Meeting*; Toulouse, France, 1990; p 127−128.

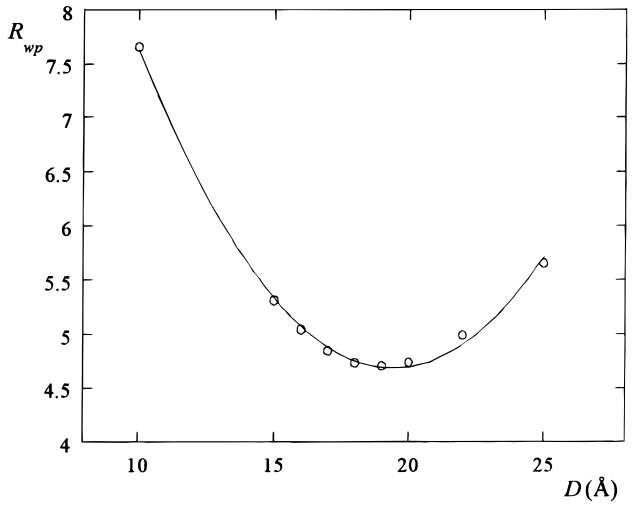

Figure 1. R_{wp} profile factor versus crystallite diameter obtained from pattern modeling of hydrated ceria $CeO_2 \cdot 1.6H_2O$ for spherical nanocrystallites in the size range 10−25 Å.

in Figure 1 by the changes of the R_{wp} factors with the diameter of the crystallites. The minimum is reached for crystallites with a diameter of 19 Å. The corresponding Rietveld plot is shown in Figure 2. The final refined parameter $a = 5.428(7)$ Å agrees, within 3 esd's, with the value reported for CeO_2 by NBS.[13] The study demonstrates that the precursor $CeO_2 \cdot 1.6H_2O$ has the crystal structure of CeO_2 and, then, is an oxide with adsorbed water molecules. The high background level is due to diffraction line broadening and to diffuse scattering arising from the adsorbed water molecules on the surface of the nanocrystallites of CeO_2. The procedure described here for estimating the crystallite size of $CeO_2 \cdot 1.6H_2O$ is approximate, since it is assumed that microstrains are negligible (which is likely to be true from the results discussed in the next section) and that a distribution of crystallite sizes and an instrumental contribution have been ignored. Nevertheless, the dominant broadening effect is obviously crystallite size, as shown by the breadth of the line 111, $\text{fwhm}_{111} = 6°\ 2\theta$ at 28.5° 2θ, which is considerably broader with respect to the instrumental resolution function (∼0.06° 2θ).

3.2. Crystallite Size and Shape of *sul*-CeO_2 and *am*-CeO_2 and Isothermal Crystallite Growth. *A. Early Stages of Crystallite Growth.* An example of whole powder pattern modeling for *sul*-CeO_2 obtained at 700 °C is shown in Figure 3. The microstructure of seven samples of *sul*-CeO_2 and *am*-CeO_2 annealed isothermally in the temperature ranges 600−900 and 550−775 °C, respectively, were analyzed by means of the integral breadth, i.e., Williamson−Hall plots[27] and Langford plots,[17] and the Fourier (*Prof*FOU) methods.

1. Integral Breadth Method. The first step in the analysis of diffraction line breadths in terms of microstructure is to examine the Williamson−Hall plots (β_f^* versus d^*) obtained for the seven samples of *sul*-CeO_2 and *am*-CeO_2. They are shown in Figure 4. It is immediately apparent that there is very little scatter in the values of β_f^* from straight lines, which is indicative on average of isotropic microstructural properties, except for the sample of *am*-CeO_2 obtained at the lowest temperatures (550 °C). For each sample *sul*-CeO_2, β_f^* is the same, to within the experimental error, for all reflections of a pattern, indicating that there is not a measurable contribution from microstrains. For *am*-CeO_2, at low temperatures (550−650 °C) the straight lines have a slight nonzero slope, whose magnitude decreases with temperature. In these few cases, there is an appreciable crystallite size effect and the scatter of breadths could be due to anisotropic sizes or, more likely, to a small contribution from microstrain with an apparent lattice direction dependence. It is beyond the scope of this study dealing mainly with crystallite sizes to proceed to a detailed analysis of microstrains and order-dependent effects in these few *am*-CeO_2 samples. Clearly, apart from a lower precision, the origin of the scatter of the integral breadths in *am*-CeO_2 (550 °C) is probably due to the presence of a dislocation structure in the sample.[28] However, separation of these size and strain quantities can be carried out by the average size−strain analysis of Langford.[17] This is illustrated in Figure 5 by the Langford plot $[(\beta_f^*/d^*)^2$ versus $\beta_f^*/(d^*)^2]$ for *am*-CeO_2 (550 °C). The slope is the reciprocal of ϵ_β and the intercept is approximately $(5e_{rms}/2)^2$, where e_{rms} is the rms strain. The same procedure was applied to all *am*-CeO_2 samples. The results obtained from the integral breadth method for the samples *sul*-CeO_2 and *am*-CeO_2 are given in Table 1. Since the size effect appears as isotropic, all average apparent sizes have

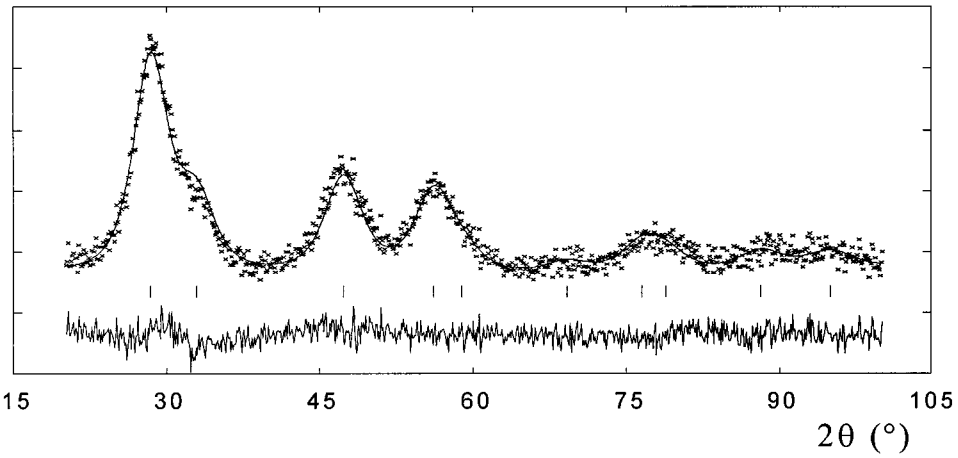

Figure 2. Rietveld refinement plot of $CeO_2 \cdot 1.6H_2O$ with spherical crystallites of 19 Å diameter: (×) experimental data; the calculated pattern is shown by the solid line; the lower trace corresponds to the difference curve between observed and calculated patterns; the Bragg reflections are shown by the vertical bars.

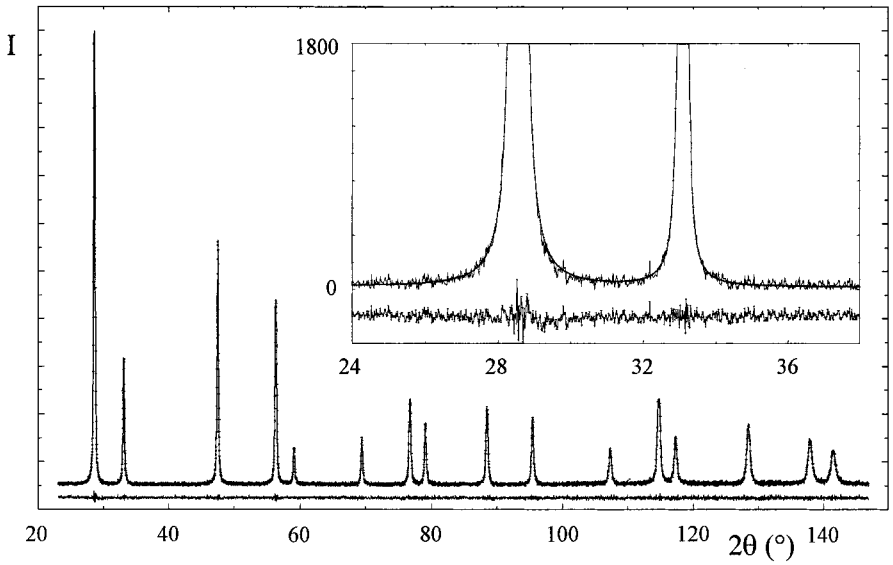

Figure 3. Whole powder pattern fitting; line profiles modeled with pseudo-Voigt functions for *sul*-CeO_2 (700 °C) obtained from three ranges (23−64°, R_{wp} = 1.86%; 64−101°, R_{wp} = 2.87%; 101−147°, R_{wp} = 2.56%). The inset shows (enlarged) the fitting of the 111 and 200 lines.

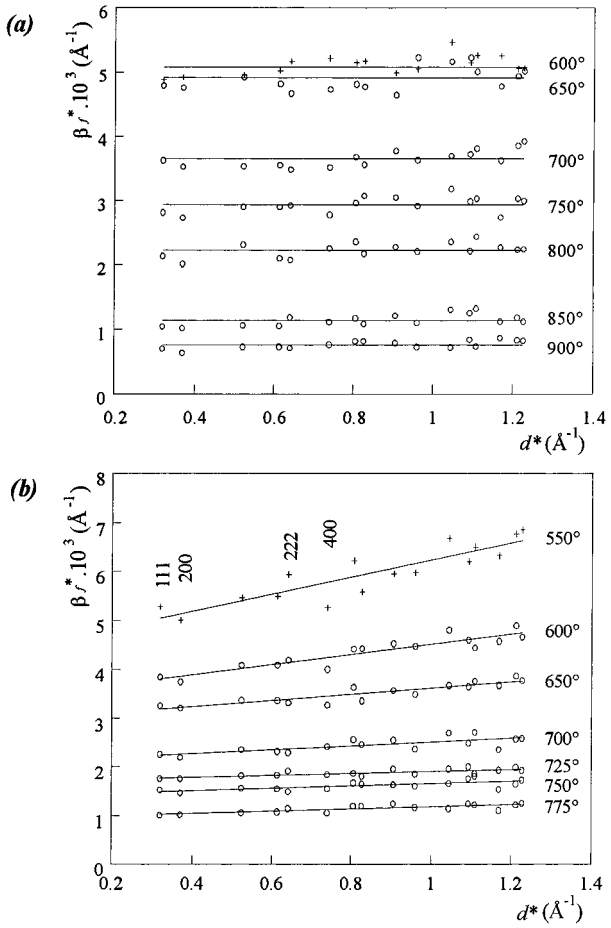

Figure 4. Williamson−Hall plots of CeO_2 prepared at various temperatures (°C): (a) *sul*-CeO_2 and (b) *am*-CeO_2. The data for the lowest temperature are displayed by pluses (+).

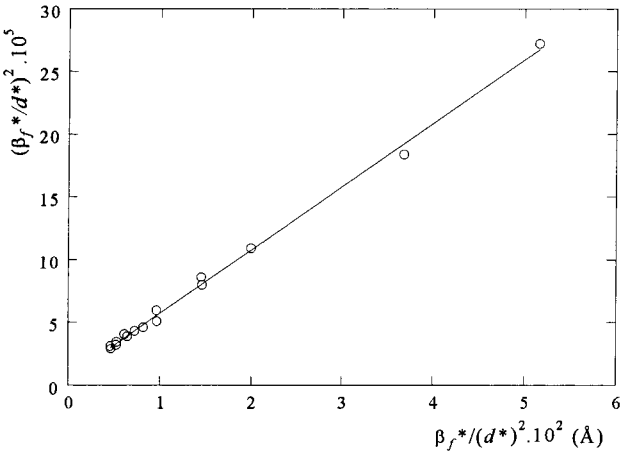

Figure 5. Langford plot for *am*-CeO_2 (550 °C).

been transformed into an average $\langle D_\beta \rangle$ (= $4\langle \epsilon_\beta \rangle/3$) calculated from all reflections in the patterns. $\langle D_\beta \rangle$ increases with the annealing temperature of CeO_2 and the microstrains e_{rms} for *am*-CeO_2 decreases rapidly with increasing temperature until to become negligeable from 700 °C.

*2. Fourier Analysis. Prof*FOU has been applied to the 16 reflections of the 7 patterns of *sul*-CeO_2 and *am*-CeO_2. The Stokes corrected Fourier coefficients $A(n,l)$ versus L are shown in Figure 6a for *sul*-CeO_2 (600 °C) and Figures 6b−d for *am*-CeO_2 (550 °C). It is immediately apparent that the 16 curves of *sul*-CeO_2 (600 °C) are, to within the experimental errors, superposed (Figure 6a), which is indicative of a strain-free oxide with spherical crystallites, on average. This is in perfect agreement with the results already described from the integral breadth method. On the other hand, there is some deviation from the superposition of all curves for *am*-CeO_2 (550 °C). In Figure 6c and 6d are shown the behavior of the $A(n,l)$ curves for two pairs of lines with different orders (111/222, 200/400) showing the presence of direction-dependent strain broadening (which is almost negligible for h00 lines). For all samples, the apparent sizes ϵ_F were estimated from the slopes at the origin of the $A(n)$ versus L plots. The procedure was also applied to *am*-CeO_2, since the size contribution is dominant and the effect of strains on the initial slope was estimated almost negligible, as seen in Figure 6c

(27) Williamson, G. K.; Hall, W. H. *Acta Metall.* **1953**, *1*, 22−31.
(28) Ungar, T. Private communication, 1999.

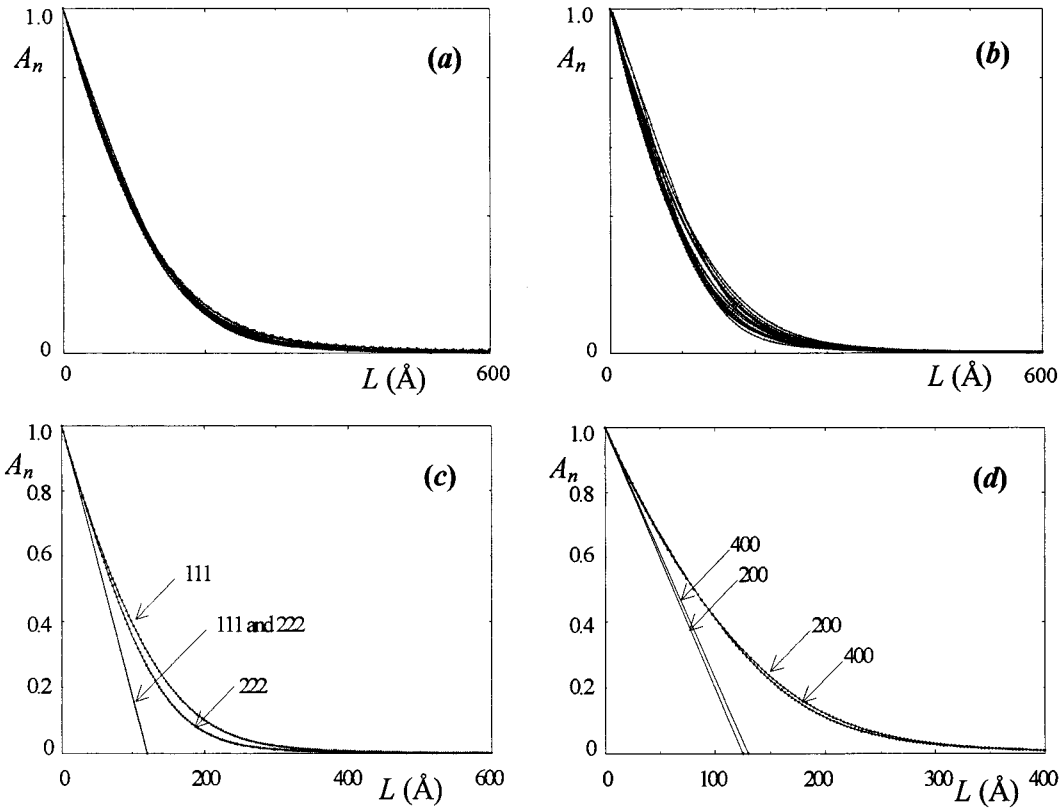

Figure 6. Cosine Fourier coefficients A_n versus L for the 16 reflections of the diffraction patterns: (a) *sul*-CeO_2 (600 °C), (b) *am*-CeO_2 (550 °C), (c) 111/222 reflections of *am*-CeO_2 (550 °C), and (d) 200/400 reflections of *am*-CeO_2 (550 °C).

Table 1. Microstructural Parameters for *sul*-CeO_2 and *am*-CeO_2 Samples (HW: Halder−Wagner Approximation)

sul-CeO_2				*am*-CeO_2				
T (°C)	$\langle D_\beta \rangle$ (Å)	$\langle D_F \rangle$ (Å)	$\langle \epsilon_\beta \rangle / \langle \epsilon_F \rangle$	T (°C)	$\langle D_\beta \rangle$ (Å)	$\langle D_F \rangle$ (Å)	$\langle \epsilon_\beta \rangle / \langle \epsilon_F \rangle$	e_{rms}
600	263(8)	195(12)	1.52	550	264(8)	178(22)	1.67	$1.1(5) \times 10^{-3}$
650	272(11)	203(20)	1.51	600	360(6)	238(21)	1.70	$8(2) \times 10^{-4}$
700	365(12)	274(18)	1.50	650	416(3)	301(24)	1.56	$5(1) \times 10^{-4}$
750	453(19)	334(21)	1.53	700	607(5)	443(33)	1.54	$4(1) \times 10^{-4}$
800	599(29)	474(42)	1.42	725	769(7)	627(33)	1.38	$2.4(7) \times 10^{-4}$
850	1167(87) (HW)	927(131)	1.42	750	901(12)	665(65)	1.52	$2.1(8) \times 10^{-4}$
900	1756(149) (HW)			775	1349(19) (HW)	1079(132)	1.41	$2.0(5) \times 10^{-4}$

and 6d. Since the size effect is again, on average, isotropic, all mean apparent sizes have been averaged to obtain a mean Fourier crystallite diameter $\langle D_F \rangle$ ($= \langle 3\epsilon_F \rangle / 2$). They are listed in Table 1 as a function of temperature.

The values of $\langle D_\beta \rangle$ and $\langle D_F \rangle$ listed in Table 1 are significantly different for each CeO_2 sample investigated, which is an indication of the presence of a distribution of crystallite sizes.[23] This is also verified from the ratio $\langle \epsilon_\beta \rangle / \langle \epsilon_F \rangle$ (Table 1), since for spherical crystallites with the same size, the ideal ratio is 1.125. They decrease slightly with temperature from 1.52 to 1.42 for *sul*-CeO_2 and 1.67 to 1.41 for *am*-CeO_2, which is indicative of a narrowing of the distributions when temperature increases.

B. Crystallite Growth Kinetics. "Particle"/crystallite growth kinetic generally follows the empirical equation:[29]

$$s^n - s_0^n = kt$$

where s is the mean "particle" size at the time t; s_0, the mean initial "particle" size; n, the kinetic "particle" growth exponent; t, the time; and k, a temperature-dependent constant. [For a process thermally activated $k = A \exp(-E_a/RT)$, where A is a constant, R is the gas constant, T is the absolute temperature, and E_a is the apparent activation energy for the growth process.] For $s \gg s_0$ and a constant crystallite growth time t, which is here the time required for a complete crystallite growth at a given temperature, the slope of the plot of ln s against $1/T$ is equal to $-E_a/nR$. In addition, the slope of the plot of ln s versus ln t provides the parameter n for a given temperature.

Crystallite growth of *am*-CeO_2 and *sul*-CeO_2 has been studied at 600 °C from TDXD. For both samples the plots of ln D versus ln t are satisfactorily fitted by straight lines (Figure 7a,b). The kinetic crystallite-growth-exponents n calculated from the slopes are 5.1(2) and 4.6(2), respectively. These close values suggest a similar crystallite growth mechanism for the CeO_2 samples obtained from the two hydrated ceria precursors. These values of n were assumed to be constant over the temperature ranges investigated.

(29) Doremus, R. H. *Rates of phase transformations*; Harcourt Brace Jovanovich: Orlando, 1985.

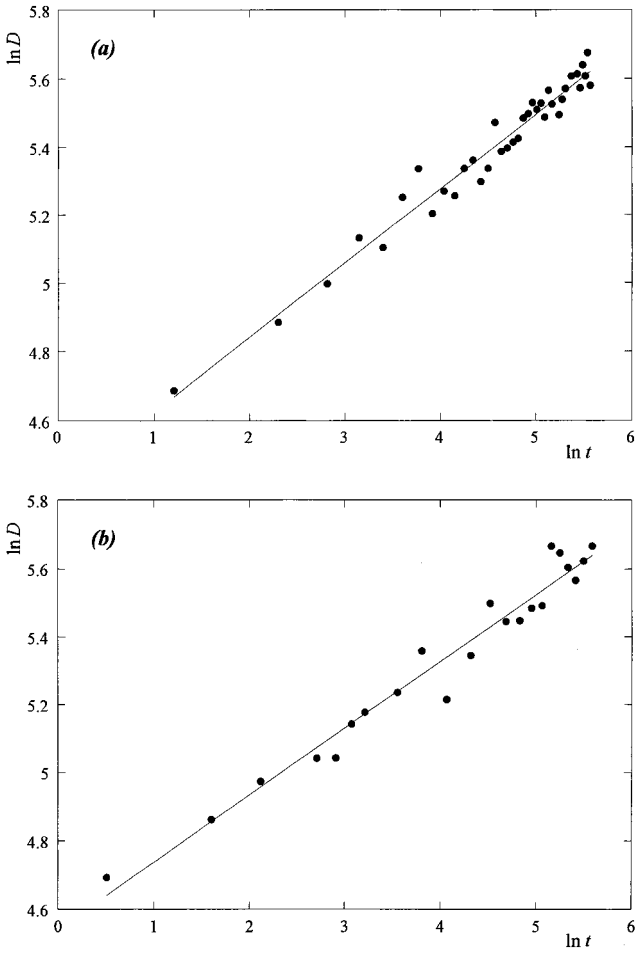

Figure 7. Plots ln D versus ln t for samples prepared at 600 °C: (a) *sul*-CeO_2 and (b) *am*-CeO_2.

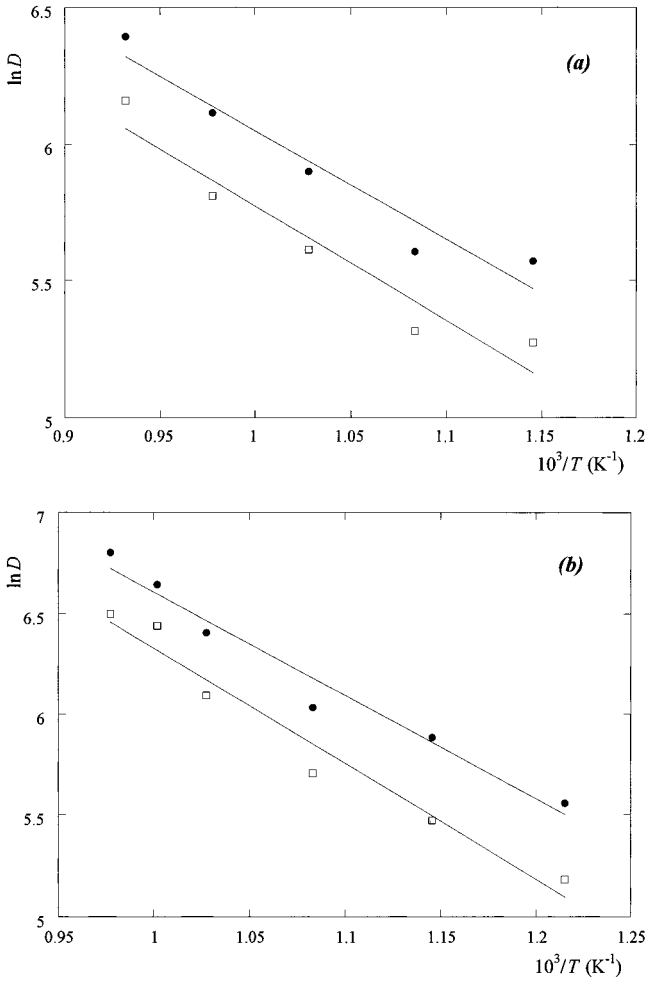

Figure 8. Plots ln D versus $1/T$ for samples prepared at constant temperatures: (a) *sul*-CeO_2 and (b) *am*-CeO_2. ●: D_β from the integral breadth method. □: D_F from the Fourier method.

Figure 8a,b shows the Arrhenius plots constructed from the data reported in Table 1 for *am*-CeO_2 and *sul*-CeO_2, in which ln $\langle D \rangle$ ($\langle D_\beta \rangle$ or $\langle D_F \rangle$) is plotted as a function of $1/T$. The values of the apparent activation energy E_a for crystallite growth, calculated from the slope of the lines and n, are given in Table 2. It can be concluded that: (i) for the two samples the E_a values obtained are similar, regardless of the line broadening analysis used and (ii) the apparent activation energy calculated for *am*-CeO_2 (mean value 231 kJ mol^{-1}) is greater than that found for *sul*-CeO_2 (mean value 157 kJ mol^{-1}). This result shows that the crystallite growth rate depends on the precursor. This is in accordance with previous observations reported for CeO_2 obtained from thermal decomposition of cerous nitrate (E_a = 46 and 203 kJ mol^{-1}), cerous oxalate (E_a = 125 kJ mol^{-1}), and ammonium ceric nitrate (E_a = 65 kJ mol^{-1}).[30] In addition, the high values of activation energy found in this study suggest that the mass-transport mechanism is likely associated with crystallite-boundary diffusion or lattice diffusion processes.

Table 2. Kinetic Parameters for the Early Stages of CeO_2 Crystallite Growth

sample	temperature range $10^3/T$ (K^{-1})	E_a (kJ mol^{-1})
sul-CeO_2	0.93−1.15	153(19)[a] 161(23)[b]
am-CeO_2	0.98−1.22	221(21)[a] 242(27)[b]

[a] Crystallite diameters estimated from the integral breadth method. [b] Estimated from the Fourier method.

C. SEM Measurements. Figures 9 and 10 show SEM micrographs of *sul*-CeO_2 (850 °C and 900 °C) and *am*-CeO_2 (550 °C and 775 °C). Figure 9a (*sul*-CeO_2) clearly shows irregular rodlike pseudomorphs of the crystal morphology of the sulfate precursor, which are comparable to those reported by Hsu et al.[8] for CeO_2 particles prepared from forced hydrolysis of concentrated ceric sulfate solutions at high pH. Figure 9b shows that these pseudomorphs are built from quasi-spherical "particles" (∼0.5−1 μm diameter at 900 °C). The "particles" of *am*-CeO_2 have no defined geometry (Figure 10a), however they are also constituted by spherical "particles" (∼100 nm diameter at 775 °C), with necks between "particles" (Figure 10b). It can be stated that the morphology of the "particles" inside the pseudomorphs is independent of the nature of the precursor and that they are spherical, on average. The "particle" size increases with the temperature. It is worthwhile to note that the sizes observed from SEM micrographs for *am*-CeO_2 compare well with the crystallite sizes calculated from X-ray diffraction methods (∼135 nm at 775 °C, Table 1), which has also been confirmed for other temperatures (e.g.,

(30) El-Adham, K. A.; Gadalla, A. M. M. *Interceram* **1977**, *3*, 223−226.

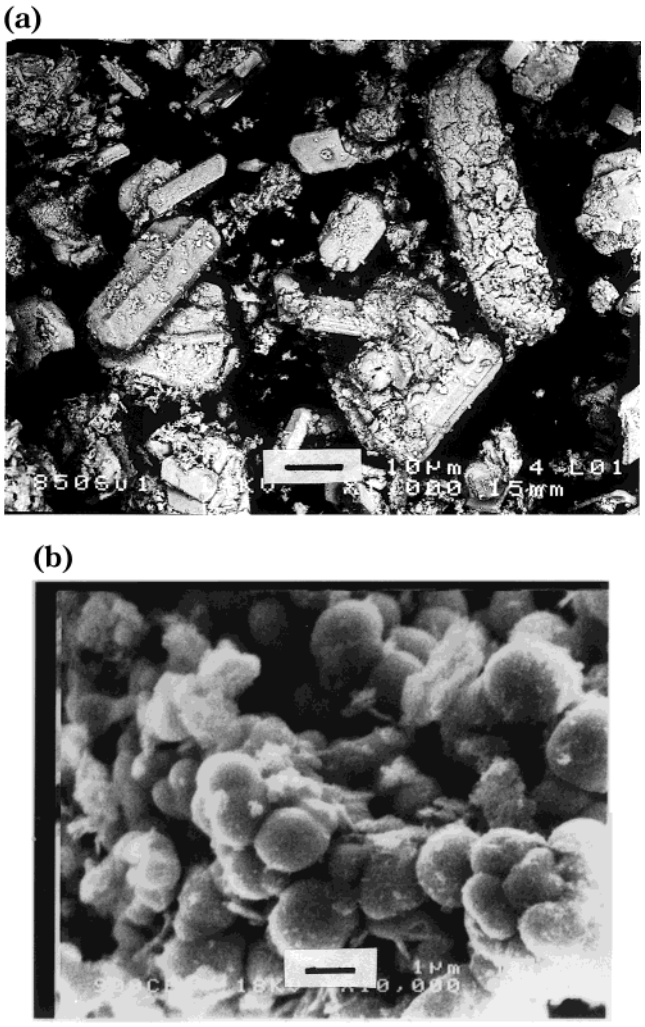

Figure 9. SEM micrographs of *sul*-CeO_2 obtained at (a) 850 °C (bar = 10 μm) and (b) 900 °C (bar = 1 μm).

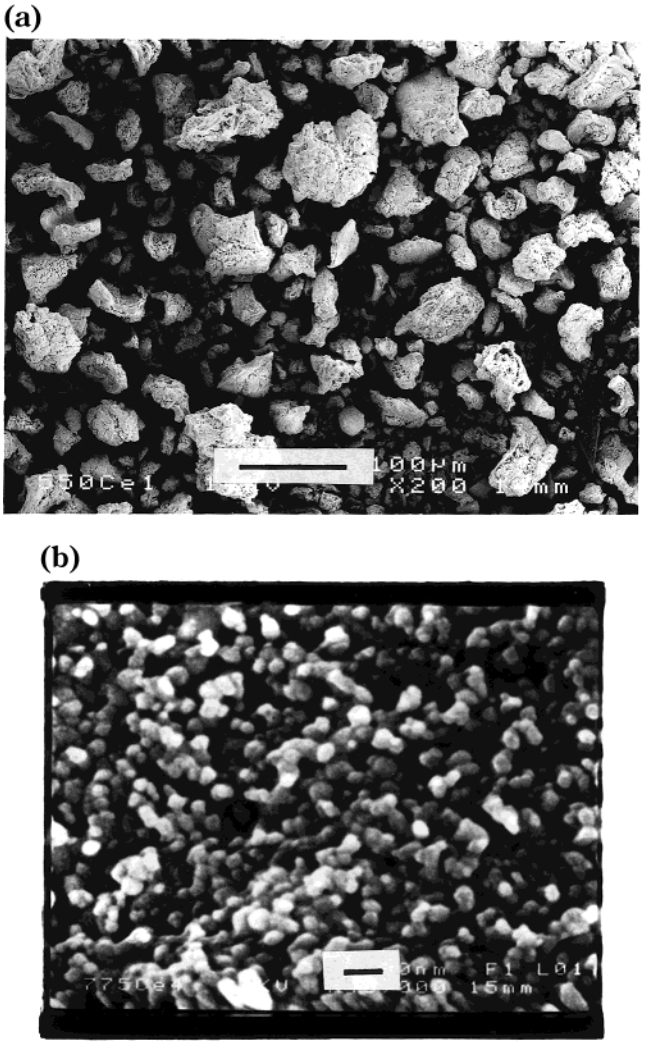

Figure 10. SEM micrographs of *am*-CeO_2 obtained at (a) 550 °C (bar = 100 μm) and (b) 775 °C (bar = 200 nm).

Table 3. Observed Surface Areas (S_{BET}), Observed "BET" Mean Diameters (D_{BET}) and Calculated Ratios $(D_{BET}/\langle D_\beta\rangle)^3$ for *sul*-CeO_2 and *am*-CeO_2

sul-CeO_2				*am*-CeO_2			
T (°C)	S_{BET} ($m^2\ g^{-1}$)	D_{BET} (Å)	$(D_{BET}/\langle D_\beta\rangle)^3$	T (°C)	S_{BET} ($m^2\ g^{-1}$)	D_{BET} (Å)	$(D_{BET}/\langle D_\beta\rangle)^3$
600	11.64	714	20	550	6.24	1332	128
650	11.93	697	17	600	5.19	1601	88
700	9.89	840	12	650	4.71	1764	76
750	9.41	883	7	700	3.60	2308	55
800	6.04	1376	12	725	3.00	2770	47
850	2.15	3865	36	750	2.98	2789	30
900	2.00	4155	13	775	2.08	3995	26

"particle" size ~30 nm and crystallite size ~26 nm at 550 °C). On the other hand, the "particle" sizes for *sul*-CeO_2 are much greater than the crystallite sizes (~180 nm at 900 °C, Table 1), which is indicative of "particles" formed from clusters of crystallites.

D. Specific Surface Area with Temperatures. The values of the specific surface areas given in Table 3 show that S_{BET} for *sul*-CeO_2 is greater than S_{BET} for *am*-CeO_2 in the annealing temperature range investigated. For the two oxides, S_{BET} decreases when the annealing temperature increases. It is worthwhile to calculate the mean BET surface area diameter (D_{BET}) for a spherical grain having the same surface area, regardless of the nature of a grain constituted by one single crystallite or several crystallites. D_{BET} was calculated from S_{BET} using the relation:

$$D_{BET} = 6 \times 10^4/(\rho S_{BET})$$

where ρ is the theoretical density of CeO_2 (7.22 g cm^{-3}) and S_{BET} is expressed in $m^2\ g^{-1}$. The calculated values of D_{BET} reported in Table 3, are always larger than the crystallite sizes (Table 1). This result suggests that crystallites are agglomerated to form grains. The average number of crystallites contributing to a grain is equal to the ratios $(D_{BET}/\langle D_\beta\rangle)^3$ listed in Table 3. It can be seen that the ratios are larger for *am*-CeO_2 than for *sul*-CeO_2. The rapid decrease of the ratio for *am*-CeO_2 with temperature reveals a competition between grain and crystallite growths in the course of annealing, i.e., the crystallite growth rate is greater than the grain growth rate. A similar feature was previously observed during the annealing of CeO_2 prepared from the thermal decomposition of the cerium oxide nitrate.[4] On the other hand, the ratio $(D_{BET}/\langle D_\beta\rangle)^3$ for *sul*-CeO_2 appears as nearly constant [mean value: ~17(9)] from 600 to 900 °C, which is indicative that crystallites and grains grow homogeneously. In addition it can be noted that for *sul*-CeO_2, D_{BET} compares well with the "particle" size observed from SEM at 900 °C (Figure 9b).

4. Conclusion

The present study on CeO_2 powders obtained from two hydrated ceria has demonstrated that the microstructural properties can be precisely determined, at the nanometer scale, from diffraction line broadening combined with modern fitting approaches. The analysis is capable of revealing subtle details about crystallite size and shape and on the nature of strain, if applicable. In this study, a three-dimensional description of crystallite shape has been reported. Clearly, the isotropic shape of the crystallites, on average, makes the analysis simpler. However, after the three-dimensional description of ZnO crystallites having the shape of cylinders[1,2] and right hexagonal prisms,[31] determined also from powder diffraction data, it is a new illustration of a precise crystallite characterization for a technologically important oxide. Similar to the early stages of crystallite growth described for ZnO[3,32,33] from line broadening analysis, the initial growth of the crystallites of CeO_2 obtained from dehydration of hydrated ceria has been carefully described at the nanometer scale, which is difficult to do from another technique. This study has demonstrated the dependence of the microstructure with the chemical nature of the precursor. Also, X-ray powder diffraction has been used to investigate samples prepared isothermally and in situ. For the two CeO_2 powders a kinetic description of crystallite growth has been discussed. In the authors' opinion, such analyses should be applied more often when studying nanocrystalline powders and should replace, as far as possible, the gross evaluation of sizes based on the fwhm of one reflection. In addition, it is clear from the structural study of nanocrystalline hydrated ceria, with sizes found as small as 19 Å, that the chemical nature of this precipitate is in fact CeO_2 with adsorbed water molecules.

As indicated in the Introduction, to our knowledge, there is no strain-free sample of CeO_2 obtained from the thermal decomposition of precursors described in the literature. In this respect *sul*-CeO_2 is quite remarkable and this feature is true for the whole temperature range investigated. Moreover, the crystallite size characterization based on all reflections of the powder diffraction pattern has clearly pointed out a spherical mean shape, whose average area- and volume-weighted diameters have been determined with a quite satisfactory precision. Determination of crystallite size is a major application of the powder diffraction method. While there are standard reference materials (SRMs) for many applications, e.g., line position, instrument sensitivity, instrument line profile and quantitative analysis, there is no reference material for crystallite size and strain broadening. There is currently such a need in the powder diffraction community.[34] It is worth noting that nanocrystalline *sul*-CeO_2 is a potential candidate for such a SRM, with a simple microstructure, i.e., strain-free and spherical crystallites, on average. As shown in this study, the size of the crystallites can be easily monitored by acting on annealing temperature and time.

Acknowledgment. The authors are indebted to G. Marsolier for his technical assistance in diffraction data collection.

CM001013E

(31) Vargas, R.; Louër, D.; Langford, J. I. *J. Appl. Crystallogr.* **1983**, *16*, 512−518.
(32) Louër, D.; Vargas, R.; Auffrédic, J.-P. *J. Am. Ceram. Soc.* **1984**, *67*, 136−141.
(33) Auffrédic, J.-P.; Boultif, A.; Langford, J. I.; Louër, D. *J. Am. Ceram. Soc.* **1995**, *78*, 323−328.
(34) Balzar, D. *IUCr Commission on Powder Diffraction, Newsletter* **1999**, *22*, 3.